TOTAL-VARIATION-REGULARIZED TENSOR RING COMPLETION FOR REMOTE SENSING IMAGE RECONSTRUCTION

Wei He[1], *Longhao Yuan*[1,2] *and Naoto Yokoya*[1]

[1] RIKEN Center for Advanced Intelligence Project (AIP), Japan

[2]Graduate School of Engineering, Saitama Institute of Technology, Japan

ABSTRACT

In recent studies, tensor ring (TR) decomposition has shown to be effective in data compression and representation. However, the existing TR-based completion methods only exploit the global low-rank property of the visual data. When applying them to remote sensing (RS) image processing, the spatial information in the RS image is ignored. In this paper, we introduce the TR decomposition to RS image processing and propose a tensor completion method for RS image reconstruction. We incorporate the total-variation regularization into the TR completion model to exploit the low-rank property and spatial continuity of the RS image simultaneously. The proposed algorithm is solved by the augmented Lagrange multiplier method and has shown the superior performance in hyperspectral image reconstruction and multi-temporal RS image cloud removal against the state-of-the-art algorithms.

Index Terms— remote sensing, reconstruction, tensor ring, total-variation, cloud removal.

1. INTRODUCTION

As a tool to investigate and understand our planet, remote sensing instruments have attracted much attention in the research field. Due to the poor weather conditions and sensor failure, RS images often suffer from information missing, such as clouds and dead pixels [1], which significantly influence the subsequent application such as recognition, classification, and detection. Therefore, it is essential to predict and reconstruct the missing information of RS images.

Up to now, many RS image reconstruction methods have been proposed, and can be classified into four categories according to the different types of complementary information: 1) spatial-based method (e.g. total variation (TV) [2], sparse and non-local regularization), 2) spectral-based method [3, 4], 3) temporal-based method [5, 6] and 4) hybrid method. The first three categories only utilize one or two kinds of prior information and are suitable for some specific cases. In order to improve the performance, it is necessary to develop hybrid methods to integrate spatial, spectral, and temporal information simultaneously [1]. Low-rank tensor completion (LRTC) is one of the smartest ways to integrate all the prior information together, which has been successfully introduced to RS image reconstruction tasks [7, 8]. By unfolding the tensor to matrices along different dimensions and minimizing the sum of all the matrices' ranks (i.e. Tucker rank minimization), the prior information of spatial, spectral and temporal information is explored simultaneously. However, the Tucker rank based LRTC methods have two drawbacks. Firstly, the Tucker rank minimization is based on an unbalanced matrix unfolding scheme (one mode versus the rest) and may not be able to describe the global information of the tensor [9, 10]. Secondly, it is far from enough to regularize the spatial prior as low-rank, because the low-rank property along the spatial dimension is not so strong in many situations [11, 12, 13].

Recently, matrix product state/tensor-train (MPS/TT) has drawn much attention due to its computational efficiency and high compression properties [14]. The main concept of TT is to decompose a high-order tensor into a set of three-order tensors. More importantly, TT rank is composed of the matrices' ranks which are formed by a well balanced matricization scheme and has the capacity to exploit the global correlation of the tensor entries [9]. However, in real applications, TT decomposition still faces several problems [15, 16]. One of them is that the TT model requires rank-1 constraints to the border decomposition factors, resulting in limited flexibility. To remedy this limitation, Zhao et al. [15] proposed the tensor ring (TR) decomposition model, which is more flexible than TT and can be regarded as the linear combination of a group of TT decompositions. TR decomposition overcomes the rank-1 constraints for the border factors, in which the factors can be circularly shifted and treated equivalently under trace operation.

The TR-based algorithms obtain the state-of-the-art performance in data compression [17] and tensor completion [16, 18]. However, most studies centralize on the mathematical analysis and algorithm development, and few works are focused on real applications. In this paper, we apply the TR decomposition to RS image completion problems and test the efficiency of TR completion compared to other tensor completion methods. Furthermore, total variation (TV) has been proved to be useful in the spatial smoothness exploration of

RS image [2, 19, 20]. Inspired by this, we embed the TV into our TR completion model to capture the global low-rank property and spatial smoothness of RS images simultaneously. The main ideas and contributions of this paper can be summarized as follows: 1) We propose a total-variation-regularized tensor ring completion (TVTRC) method for RS image reconstruction. The TR decomposition is applied to explore the low-rank information of the tensor. Meanwhile, TV is adopted to explore the spatial smoothness of the RS images. 2) The augmented Lagrangian method (ALM) algorithm is employed to solve the TVLRC model. Several experiments on hyperspectral image reconstruction and time-series image cloud removal are conducted to demonstrate the advantage of the proposed method.

2. APPROACH

2.1. Notations and Problem Formulation

We mainly adopt the notations from [21] in this paper. Tensors of order $N \geq 3$ are denoted by calligraphic letters, e.g., $\mathcal{X} \in \mathbb{R}^{I_1 \times I_2 \times \cdots \times I_N}$. Scalars are denoted by normal lowercase letters or uppercase letters, e.g., $x, X \in \mathbb{R}$. Vectors are denoted by boldface lowercase letters, e.g., $\mathbf{x} \in \mathbb{R}^{I}$. Matrices are denoted by boldface capital letters, e.g., $\mathbf{X} \in \mathbb{R}^{I \times J}$. We employ two types of tensor unfolding (matricization) operations in this paper. The first mode-n unfolding [21] of tensor $\mathcal{X} \in \mathbb{R}^{I_1 \times I_2 \times \cdots \times I_N}$ is denoted by $\mathbf{X}_{(n)} \in \mathbb{R}^{I_n \times I_1 \cdots I_{n-1} I_{n+1} \cdots I_N}$ and the second which is often used in TR operations [15] is denoted by $\mathbf{X}_{<n>} \in \mathbb{R}^{I_n \times I_{n+1} \cdots I_N I_1 \cdots I_{n-1}}$. Furthermore, matrix folding (tensorization) operation which transforms a matrix into a higher-order tensor is defined as $\text{fold}_n(\cdot)$, i.e., for a tensor $\mathcal{X}$, we have $\text{fold}_n(\mathbf{X}_{(n)}) = \mathcal{X}$. In addition, the inner product of two tensors $\mathcal{X}$, $\mathcal{Y}$ with the same size $\mathbb{R}^{I_1 \times I_2 \times \cdots \times I_N}$ is defined as $\langle \mathcal{X}, \mathcal{Y} \rangle = \sum_{i_1} \sum_{i_2} \cdots \sum_{i_N} x_{i_1 i_2 \dots i_N} y_{i_1 i_2 \dots i_N}$, and the Frobenius norm of $\mathcal{X}$ is defined by $\|\mathcal{X}\|_F = \sqrt{\langle \mathcal{X}, \mathcal{X} \rangle}$.

For the RS image reconstruction task, we adopt $\mathcal{Y}$ standing for the incomplete observed image with the set of indices of observed entries which is denoted as Ω. We aim to find the complete RS image $\mathcal{X}$ under the condition $\mathcal{X}_\Omega = \mathcal{Y}_\Omega$.

2.2. Tensor Ring Decomposition

TR decomposition represents a tensor of high-order by circular multilinear products over a sequence of three-order core tensors, i.e., TR factors. For $n = 1, \dots, N$, the TR factors are denoted by $\mathcal{G}^{(n)} \in \mathbb{R}^{R_n \times I_n \times R_{n+1}}$ where $\{R_1, R_2, \dots, R_{N+1}\}$ denotes the TR-rank which controls the model complexity of TR decomposition. Trace operations are applied in TR decomposition and this makes all of the TR factors are of size order-three, thus the rank constraint of TR decomposition is relaxed to $R_1 = R_{N+1}$. In this case, TR decomposition can be considered as a linear combination of TT decomposition, so it is a more generalized model than TT decomposition. The relation of TR factors and the generated tensor is formulated by (1):

$$\mathbf{X}_{<n>} = \mathbf{G}^{(n)}_{(2)} (\mathbf{G}^{(\neq n)}_{<2>})^T, \tag{1}$$

where $\mathcal{G}^{(\neq n)} \in \mathbb{R}^{R_{n+1} \times \prod_{i=1, i \neq n}^{N} I_i \times R_n}$ is a subchain tensor by merging all but the n-th core tensor, see details in [22].

2.3. Proposed TVTRC

We firstly develop the tensor completion model on the basis of TR decomposition, and subsequently incorporate the TV regularization into the TR completion to explore the spatial, spectral and temporal information of RS image simultaneously. The TR completion can be formulated as follows

$$\min_{\mathcal{X}, \mathcal{G}} \|\mathcal{X} - \Phi(\mathcal{G})\|_F^2, \ s.t. \ \mathcal{X}_\Omega = \mathcal{Y}_\Omega, \tag{2}$$

where $\mathcal{G} := \{\mathcal{G}^{(1)}, \dots, \mathcal{G}^{(N)}\}$, Φ is the operater to transform the TR factors into the approximated tensor. The TR-rank is reflected by the size of $\mathcal{G}^{(n)} \in \mathbb{R}^{R_n \times I_n \times R_{n+1}}$ and allocated in advance.

When model (2) is adopted to the reconstruction of RS image, only the low-rank property of the image would be explored. As pointed out in [11], the low-rank property of the spatial mode of the RS image is weak, and not enough to describe the spatial information. From another aspect, the adjacent pixels have a strong correlation, indicating the spatial piecewise smoothness structure. Inspired by this fact, we embed the TV regularization into the TR completion model to combine the low-rank property and spatial smoothness structure together. The proposed TVLRC model is formulated as:

$$\min_{\mathcal{X}, \mathcal{G}} \lambda \|\mathcal{X}\|_{TV} + \|\mathcal{X} - \Phi(\mathcal{G})\|_F^2, \ s.t., \ \mathcal{X}_\Omega = \mathcal{Y}_\Omega, \tag{3}$$

where $\|\mathcal{X}\|_{TV} = \sum_{i_3, \dots, i_N}^{I_3, \dots, I_N} \|D_x(\mathcal{X}(:,:,i_3,...,i_N))\|_1 + \|D_y(\mathcal{X}(:,:,i_3,...,i_N))\|_1$ standing for the spatial TV along all spectral and temporal dimensions, and $D = [D_x, D_y]$ represent the first-order discrete differences from horizontal and vertical perspective, $\|\cdot\|_1$ is the 1-norm regularization. Parameter λ is the weight of TV regularization and set as 10^{-2} in the paper.

2.4. Optimization

In this part, we apply the ALM algorithm to solve the model (3). We first introduce an auxiliary variable $\mathcal{U}$ and obtain the following optimization model

$$\begin{aligned} \min_{\mathcal{X}, \mathcal{G}, \mathcal{U}} & \lambda \|\mathcal{U}\|_1 + \|\mathcal{X} - \Phi(\mathcal{G})\|_F^2 + \langle \Lambda, \mathcal{U} - D\mathcal{X} \rangle \\ & + \frac{\mu}{2} \|\mathcal{U} - D\mathcal{X}\|_F^2, \ s.t. \ \mathcal{X}_\Omega = \mathcal{Y}_\Omega. \end{aligned} \tag{4}$$

Here, Λ stands for the Lagrange multiplier and μ is the penalty parameter.

For the update of variables, we firstly fix $\boldsymbol{\mathcal{X}}$ and $\boldsymbol{\mathcal{U}}$, and update $\boldsymbol{\mathcal{G}}$. For $n = 1, \ldots, N$, the optimization is:

$$\boldsymbol{\mathcal{G}}^{(n)} = \text{fold}_2(\boldsymbol{\mathcal{X}}_{<n>}(\mathbf{G}^{(\neq n)}_{<2>})^{T,\dagger}), \tag{5}$$

where $\dagger$ is the Pseudo-inverse of the matrix.

Secondly, fix $\boldsymbol{\mathcal{G}}$ and $\boldsymbol{\mathcal{U}}$, and update $\boldsymbol{\mathcal{X}}$. The fast Fourier transform (FFT) is adopted to solve the subproblem

$$\boldsymbol{\mathcal{X}} = \boldsymbol{\mathcal{F}}^{-1}\left[\frac{\boldsymbol{\mathcal{F}}(\Phi(\boldsymbol{\mathcal{G}}) + D^T(\mu\boldsymbol{\mathcal{U}} + \Lambda)/2)}{1 + (\boldsymbol{\mathcal{F}}(\mu D_x/2))^2 + (\boldsymbol{\mathcal{F}}(\mu D_y/2))^2}\right]. \tag{6}$$

We set $\boldsymbol{\mathcal{X}}_\Omega = \boldsymbol{\mathcal{Y}}_\Omega$ to keep the observed values unchanged. Thirdly, fix $\boldsymbol{\mathcal{G}}$ and $\boldsymbol{\mathcal{X}}$, and update $\boldsymbol{\mathcal{U}}$. It is equivalent to solve

$$\min_{\boldsymbol{\mathcal{U}}} \lambda\|\boldsymbol{\mathcal{U}}\|_1 + \frac{\mu}{2}\|\boldsymbol{\mathcal{U}} - \boldsymbol{\mathcal{X}} + \Lambda/\mu\|_F^2, \tag{7}$$

which can be solved by soft-thresholding (shrinkage) operator [19].

Finally, the Lagrange multiplier Λ is updated by

$$\Lambda = \Lambda + \mu(\boldsymbol{\mathcal{U}} - \boldsymbol{\mathcal{X}}), \tag{8}$$

where μ is updated by the strategy in [20].

3. EXPERIMENTS AND DISCUSSION

3.1. Data description

RS datasets were adopted in our experiments. The first one was the Washington DC (WDC) Mall dataset from HYDICE sensor [23]. We select a sub-image of size $256 \times 256 \times 30$ from the original image for the simulated reconstruction experiments with random missing. In the experiments, the simulated random missing percentage of the WDC image was from 50%, 70% to 90%. The second dataset was the one-year time-series Sentinel-2 images from the Tokyo area[1]. The time-series image tensor is of size $400 \times 400 \times 4 \times 15$, which means spatial size 400×400, spectral bands number 4 and 15 time nodes. The dataset is clean and free from the clouds. We added the simulated clouds to conduct the simulated cloud removal experiments. The third dataset was also the one-year time-series Sentinel-2 image from Tokyo area with size $400 \times 400 \times 4 \times 15$. The dataset is corrupted by the real clouds and adopted for the real cloud removal experiment.

For TRALS and the proposed TVTRC, the rank was set as $[15, 15, 10]$ for the hyperspectral image reconstruction and $[15, 15, 3, 5]$ for the time-series cloud removal.

Several existed methods were selected for comparison, including adaptive weighted LRTC (AWTC) [8], tensor completion using TV and low-rank matrix factorization (TVMF) [24], TT completion with Stochastic Gradient Descent (TTSGD) [25], and TR completion with Alternating Least Square (TRALS) [16]. For the real could removal experimental results, Fmask [26] was adopted to detect the cloud and cloud shadow location.

For the simulated data experiments, we adopted the peak signal-to-noise ratio (PSNR) and the structural similarity (SSIM) to evaluate the results. For hyperspectral and time-series images, we calculated the values of PNSR and SSIM of each band and then average them [20].

Table 1. Quantitative evaluation of simulated data experiments for hyperspectral image reconstruction with random missing of 50%, 70%, and 90% and time-series image cloud removal.

Missing	index	AWTC	TVMF	TTSGD	TRALS	TVTRC
50%	PSNR(dB)	50.41	37.93	38.15	52.56	**52.96**
	SSIM	0.998	0.950	0.965	0.998	**0.999**
70%	PSNR(dB)	45.91	31.85	34.82	49.78	**50.36**
	SSIM	0.993	0.875	0.929	0.997	**0.997**
90%	PSNR(dB)	27.63	29.19	28.01	35.63	**36.40**
	SSIM	0.781	0.776	0.721	0.934	**0.951**
cloud Removal	PSNR(dB)	**45.36**	42.38	43.61	43.12	45.05
	SSIM	0.945	0.896	0.940	0.912	**0.950**

3.2. Simulated data experiments

The quantitative evaluation results with simulated data for the hyperspectral image random missing reconstruction and the time-series image cloud removal are presented in Table 1. From the table, it can be easily observed that the proposed TVLRC achieved the highest PSNR and SSIM values in the hyperspectral image random missing reconstruction. When the missing percentage is low, TVTRC obtained a bit higher accuracy than those of AWTC and TRALS. However, when the missing percentage increases, the performance of TVTRC is much better than that of the other two methods. The color images, extracted from the hyperspectral image, before and after reconstruction presented in Fig. 1 also confirm the advantage of the proposed method in the highly missing situation. From another aspect, TTSGD and TVMF achieved better results in the highly missing situation, meanwhile performed worse in the low missing case. In the simulated cloud removal experiments, AWTC achieved the highest PSNR values. Meanwhile, the proposed TVTRC obtained the highest SSIM value. From the visual results presented in the second row of Fig. 1, the proposed method presents the best reconstructed details compared to other comparison methods.

3.3. Real data experiment

Fig. 2 presents one time node color images of real data experiments before and after reconstruction. Fig. 2(a) stands for the real image, and Fig. 2(b) shows the mask with the white color standing for the observed area. Fig. 2(c-g) represent the reconstruction results with different methods. In the enlarged area marked in the yellow rectangle, it can be easily observed that AWTC, TVMF and TTSGD failed to restore the image

[1] download website:https://scihub.copernicus.eu/dhus/

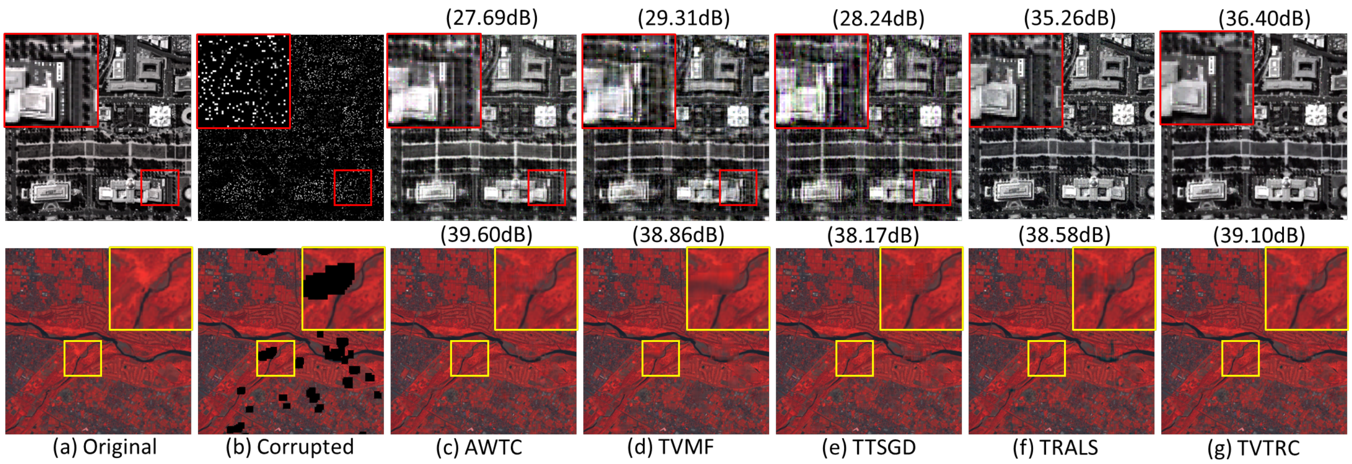

Fig. 1. Experimental results on simulated data. The first row presents the color images composed of hyperspectral band 16, 17 and 20 before and after reconstruction. The second row shows the sixth time node image of time series images.

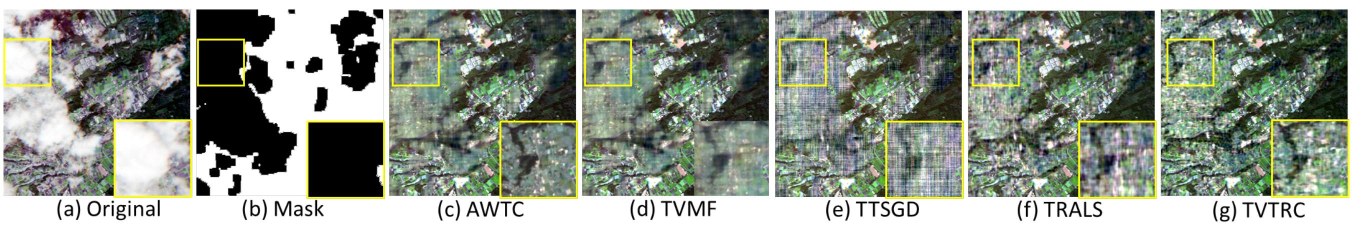

Fig. 2. Comparison of cloud removal results for the eighth time node image of real data. The red, green and blue bands are used for the color composite.

in the most area. TRALS can more or less recover the cloudy image. However, it also remained large areas to not be recovered. To sum all, the proposed TVTRC achieved the best results from the visual perspective.

4. CONCLUSION

In this paper, we introduced the TR decomposition into the remote sensing image reconstruction and proposed a total-variation-regularized tensor ring completion method (TVTRC). The TR decomposition is used to explore the spatial, spectral and temporal information simultaneously, and the total variation is adopted to further explore the spatial smoothness in RS images. The proposed TVTRC had been proved to achieve the best performance compared to other tensor completion based methods. Despite the good performance achieved by TVTRC, it still faces some drawbacks for future research. Firstly, the rank of the TR decomposition has much influence for the performance and computational efficiency. How to automatically estimate the rank is a key problem. Secondly, the calculation of TR decomposition is extremely expensive. How to improve the efficiency of TR decomposition is another key problem.

5. REFERENCES

[1] Huanfeng Shen, Xinghua Li, Qing Cheng, Chao Zeng, Gang Yang, Huifang Li, and Liangpei Zhang, "Missing information reconstruction of remote sensing data: A technical review," *IEEE Geoscience and Remote Sensing Magazine*, vol. 3, no. 3, pp. 61–85, 2015.

[2] Leonid I Rudin, Stanley Osher, and Emad Fatemi, "Nonlinear total variation based noise removal algorithms," *Physica D: nonlinear phenomena*, vol. 60, no. 1-4, pp. 259–268, 1992.

[3] Huanfeng Shen, Xinghua Li, Liangpei Zhang, Dacheng Tao, and Chao Zeng, "Compressed sensing-based inpainting of aqua moderate resolution imaging spectroradiometer band 6 using adaptive spectrum-weighted sparse bayesian dictionary learning," *IEEE Transactions on Geoscience and Remote Sensing*, vol. 52, no. 2, pp. 894–906, 2014.

[4] David P Roy, Junchang Ju, Philip Lewis, Crystal Schaaf, Feng Gao, Matt Hansen, and Erik Lindquist, "Multi-temporal modis–landsat data fusion for relative radio-

metric normalization, gap filling, and prediction of landsat data," *Remote Sensing of Environment*, vol. 112, no. 6, pp. 3112–3130, 2008.

[5] Salvador Gabarda and Gabriel Cristobal, "Cloud covering denoising through image fusion," *Image and Vision Computing*, vol. 25, no. 5, pp. 523–530, 2007.

[6] Jialei Wang, Peder A Olsen, Andrew R Conn, and Aurélie C Lozano, "Removing clouds and recovering ground observations in satellite image sequences via temporally contiguous robust matrix completion," in *Proceedings of the IEEE Conference on Computer Vision and Pattern Recognition*, 2016, pp. 2754–2763.

[7] Teng-Yu Ji, Naoto Yokoya, Xiao Xiang Zhu, and Ting-Zhu Huang, "Nonlocal tensor completion for multitemporal remotely sensed images' inpainting," *IEEE Transactions on Geoscience and Remote Sensing*, 2018.

[8] Michael Kwok-Po Ng, Qiangqiang Yuan, Li Yan, and Jing Sun, "An adaptive weighted tensor completion method for the recovery of remote sensing images with missing data," *IEEE Transactions on Geoscience and Remote Sensing*, vol. 55, no. 6, pp. 3367–3381, 2017.

[9] Johann A Bengua, Ho N Phien, Hoang Duong Tuan, and Minh N Do, "Efficient tensor completion for color image and video recovery: Low-rank tensor train," *IEEE Transactions on Image Processing*, vol. 26, no. 5, pp. 2466–2479, 2017.

[10] Hongyan Zhang, Wei He, Liangpei Zhang, Huanfeng Shen, and Qiangqiang Yuan, "Hyperspectral image restoration using low-rank matrix recovery," *IEEE Trans. Geosci. Remote Sens.*, vol. 52, no. 8, pp. 4729–4743, Aug. 2014.

[11] Yi Chang, Luxin Yan, and Sheng Zhong, "Hyper-laplacian regularized unidirectional low-rank tensor recovery for multispectral image denoising," in *Proc. IEEE Conf. CVPR*, 2017, pp. 4260–4268.

[12] Dimitris G Chachlakis and Panos P Markopoulos, "Novel algorithms for exact and efficient l1-norm-based tucker2 decomposition," in *2018 IEEE International Conference on Acoustics, Speech and Signal Processing (ICASSP)*. IEEE, 2018, pp. 6294–6298.

[13] Yu Zhang, Guoxu Zhou, Jing Jin, Minjue Wang, Xingyu Wang, and Andrzej Cichocki, "L1-regularized multiway canonical correlation analysis for ssvep-based bci," *IEEE transactions on neural systems and rehabilitation engineering*, vol. 21, no. 6, pp. 887–896, 2013.

[14] Ivan V Oseledets, "Tensor-train decomposition," *SIAM Journal on Scientific Computing*, vol. 33, no. 5, pp. 2295–2317, 2011.

[15] Qibin Zhao, Guoxu Zhou, Shengli Xie, Liqing Zhang, and Andrzej Cichocki, "Tensor ring decomposition," *arXiv preprint arXiv:1606.05535*, 2016.

[16] Wenqi Wang, Vaneet Aggarwal, and Shuchin Aeron, "Efficient low rank tensor ring completion," *Rn*, vol. 1, no. r1, pp. 1, 2017.

[17] Qibin Zhao, Masashi Sugiyama, and Andrzej Cichocki, "Learning efficient tensor representations with ring structure networks," *arXiv preprint arXiv:1705.08286*, 2017.

[18] Longhao Yuan, Chao Li, Danilo Mandic, Jianting Cao, and Qibin Zhao, "Rank minimization on tensor ring: A new paradigm in scalable tensor decomposition and completion," *arXiv preprint arXiv:1805.08468*, 2018.

[19] Wei He, Hongyan Zhang, and Liangpei Zhang, "Total variation regularized reweighted sparse nonnegative matrix factorization for hyperspectral unmixing," *IEEE Transactions on Geoscience and Remote Sensing*, vol. 55, no. 7, pp. 3909–3921, 2017.

[20] Wei He, Hongyan Zhang, Liangpei Zhang, and Huanfeng Shen, "Total-variation-regularized low-rank matrix factorization for hyperspectral image restoration," *IEEE Trans. Geosci. Remote Sens.*, vol. 54, no. 1, pp. 178–188, Jan. 2016.

[21] Tamara G Kolda and Brett W Bader, "Tensor decompositions and applications," *SIAM review*, vol. 51, no. 3, pp. 455–500, 2009.

[22] Qibin Zhao, Masashi Sugiyama, Longhao Yuan, and Andrzej Cichocki, "Learning efficient tensor representations with ring structure networks," 2018.

[23] David Landgrebe, "Hyperspectral image data analysis," *IEEE Signal Processing Magazine*, vol. 19, no. 1, pp. 17–28, 2002.

[24] Teng-Yu Ji, Ting-Zhu Huang, Xi-Le Zhao, Tian-Hui Ma, and Gang Liu, "Tensor completion using total variation and low-rank matrix factorization," *Information Sciences*, vol. 326, pp. 243–257, 2016.

[25] Qibin Zhao, Longhao Yuan, and Jianting Cao, "High-dimension tensor completion via gradient-based optimization under tensor-train format," *arXiv preprint arXiv:1804.01983*, 2018.

[26] Zhe Zhu, Shixiong Wang, and Curtis E Woodcock, "Improvement and expansion of the fmask algorithm: Cloud, cloud shadow, and snow detection for landsats 4–7, 8, and sentinel 2 images," *Remote Sensing of Environment*, vol. 159, pp. 269–277, 2015.